Effects of heat input on the mechanical properties of butt-welded high and ultra-high strength steels

Amraei Mohsen, Ahola Antti, Afkhami Shahriar, Björk Timo, Heidarpour Amin, Zhao Xiao-Ling

DOI: 10.1016/j.engstruct.2019.109460

Contents lists available at ScienceDirect

Engineering Structures

journal homepage: http://ees.elsevier.com

Effects of heat input on the mechanical properties of butt-welded high and ultra-high strength steels

Mohsen Amraei[a,b], Antti Ahola[b], Shahriar Afkhami[b], Timo Björk[b], Amin Heidarpour[c], Xiao-Ling Zhao[a,*]

[a] The School of Civil and Environmental Engineering, UNSW Sydney, NSW 2052, Australia
[b] Laboratory of Steel Structures, LUT University, P.O. Box 20, 53851 Lappeenranta, Finland
[c] Department of Civil Engineering, Monash University, Melbourne, VIC 3800, Australia

ARTICLE INFO

Keywords
High strength steel
Ultra-high strength steel
Welding
GMAW
Laser welding
Heat input
Mechanical properties
Microstructure

ABSTRACT

In this study, the mechanical properties of butt-welded thin plates made of S700, S960 and S1100 steels under various heat inputs (HI) are investigated. The gas metal arc welding (GMAW) process with two different levels of HI, and laser welding (LW) are implemented for this purpose. Fully automated welding process is employed to attain high quality and homogeneous weldments. Standard tensile tests of the butt-welded joints, together with micro-hardness measurements are conducted in this study. The microstructure of the heat affected zones (HAZ) of the weldments are closely examined using scanning electron microscopy (SEM). It was observed that while the fracture was occurred at the base materials of all S700 and S1100 weldments, the S960 suffered from failure at the HAZ which resulted in reduction of the joint's strength and ductility. For all the studied steels, it was found that the joint's ductility is highly dependent on HI values over the range of 0.3–1.4 kJ/mm for each welding pass. Though, the S1100 steel showed the best performance under welding HI with a moderate change in its mechanical properties and a stable microstructure after welding compared to S700 and S960.

1. Introduction

The application of high and ultra-high strength steels (HSS/UHSS) leads to build structures and components which are thinner, lighter yet stronger. Besides, HSS/UHSS may reduce the carbon footprint associated with its manufacturing by lowering the global steel's net production volume, and the carbon emission due to the transportation of such heavy material. Cost-effectiveness for end users is another benefit which could be gained by weight saving in the structure [1,2]. The aforementioned advantages encourage variety of engineering sectors particularly construction [2–7], and automotive industry [8–10], to continuously look for the new applications of higher grades of steel. The available common manufacturing methods to produce HSS/UHSS are quenching and tempering (Q&T), and direct quenching (DQ) [11].

Even though these grades of steel have been in the market for several decades, the terminology of HSS/UHSS is not well established yet due to the continuous developments of such steel grades [12]. According to the current definition of HSS/UHSS, advanced high strength steels with nominal yield strength up to 700 MPa are to be considered as HSS, while higher yield strengths are categorized as UHSS [13]. The current specifications such as Eurocode 3 [14], and ANSI/AISC 360-10 [15] are also limited to steels with nominal yield strengths up to 700 MPa and 690 MPa, respectively, which are HSS grades.

Besides the lack of a proper design code, HSS/UHSS are more prone to the negative effects of heat input (HI) from welding and post welding treatments [16], fire and other heat based processes compared to conventional lower grades of steel [17,18]. Welding "specifically" as the most common method to join metallic materials exposes the steel to a high amount of heat. Various welding methods are studied in the literature to join HSS/UHSS. These methods are exemplified by the laser welding (LW) of S960 grade [19–21], the gas metal arc welding (GMAW) [22,23], laser gas-metal-arc hybrid welding [24], and tungsten inert gas welding [25]. Several issues associated with the welded HSS/UHSS are reported in the literature including cold cracking [26], reduction in the load carrying capacity [16], lower fracture toughness [27–29] and lack of ductility [18].

It has been demonstrated that welding HI and cooling rate are the key parameters affecting the joint's capacity, ductility and toughness [19,20]. Due to the differences in the cooling rates at vicinity of the joint, the local heating creates a range of materials with different characteristics depending on their distance from the weld fusion zone. Among these regions, the softening at the heat-affected zone (HAZ) is the most crucial [17,19,20]. By reducing the HI and accelerating the cooling rate, it is possible to control the microstructure of the HAZ, es-

* Corresponding author.
Email address: xiaolin.zhao@unsw.edu.au (X-L Zhao)

https://doi.org/10.1016/j.engstruct.2019.109460
Received 5 March 2019; Received in revised form 5 June 2019; Accepted 28 July 2019
Available online xxx
0141-0296/

pecially at the softened region, hence to reach higher joint capacity and ductility. Farrokhi et al. [19] demonstrated that it is possible to receive a very narrow HAZ by applying a concentrated laser beam with high power and high welding speed, which results in satisfactory joint characteristics of welded DQ S960. Nevertheless, 20% reduction in the hardness values at the softened HAZ was reported in their study [19]. Amraei et al. [20] showed that the material surrounding a very narrow HAZ creates a hydrostatic stress by the means of constraint boundary condition, which increases both the joint strength and ductility. Even though they reported 25% reduction in the hardness values at the softened HAZ when 9 mm thick DQ S960 was laser welded, yet a higher strength and ductility was achieved due to this effect [20]. The reduction in hardness value is different to that of the welded UHSS tubes with yield strength of 1350 MPa as reported in [30], which shows 60% reduction at the softened HAZ.

The aforementioned investigations in the literature focus on a certain grade of HSS/UHSS, with a specific manufacturing type. However, to the knowledge of authors, no research was found to answer the question "what are the effects of HI and cooling rate on the mechanical properties of various grades of HSS/UHSS with different manufacturing history?" This research aims to answer this question by the means of detailed experimental tests. Accordingly, the steel plates made of S700, S960 and S1100 were butt-welded (BW) with various HIs. Two different welding processes were implemented to join the steel plates: the GMAW, and the LW. For the GMAW, two different welding speeds were used which stand for high and low HIs, HQ and LQ, respectively. The GMAW specimens were welded using a matching filler material as recommended in the literature [20]. For the LW, a 9 kW focused fiber laser with moving head speed of 30 mm/s was utilized. No filler material was used for the LW specimen.

2. Materials

The mechanical properties of three different steel plates (i.e. S700, S960 and S1100) with nominal thickness of 8 mm were studied in this paper. Among the aforementioned steels, S700 and S1100 are Q&T types of steel, while S960 is manufactured via DQ method. DQ can be applied in both hot strip and plate mills to produce structural and abrasion-resistant steels [11]. DQ consists of thermomechanical rolling followed by immediate water quenching and possible tempering. In DQ water quenching is done immediately after hot rolling from a temperature at which austenite is either recrystallized or non-recrystallized depending on the composition of the steel and the rolling pass schedule prior to quenching [11]. Cost reductions in comparison to conventional quenching and tempering techniques come from avoidance of the necessity for reheating, and lower alloying. The microstructure of DQ UHSS has a combination of auto-tempered or tempered lath martensite and/or bainite [20]. The nominal chemical composition of the base materials (BM) as provided by the manufacturer are listed in Table 1.

Carbon equivalent content (CEV) is calculated according to [31]:

$$\begin{aligned} CEV &= C + Mn/6 \\ &\quad + (Cr + Mo \\ &\qquad + V)/5 \\ &\quad + (Ni \\ &\qquad + Cu)/15 \end{aligned}$$

The monotonic mechanical properties of the studied steels are presented in Table 2, which are based on the manufacturer's certificate.

In order to study the effect of different HI levels on the mechanical properties and microstructure characteristics of weldments made of HSS/UHSS, the plates were joint together using the GMAW and LW. For the GMAW, two different filler materials were used including Union Ni 2.5 (wire diameter of 1.0 mm), and Union X96 (wire diameter of 1.0 mm). Union Ni 2.5 is used to weld S700 steel plates, while S960 and S1100 are welded using Union X96. The aforementioned filler materials create a weldment in the state of matching strength with the BM. Even though the nominal yield and ultimate strengths seem to be lower than the virgin base plates, the previous experiments show that these filler materials create matching joints after reheating and dilution with the base material [12,20]. The chemical compositions and mechanical properties of the filler materials are presented in Table 3. Since the LW process does not use any filler material, thus the weldment is in the state of perfect matching.

Scanning electron microscopy (SEM) of the materials used in this study is shown in Fig. 1. BMs and the used filler materials have a mixture of bainite and martensite in their microstructure.

3. Experimental tests

3.1. Test specimen

In order to determine the mechanical properties of welded high and ultra-high strength structural steels under various HIs, standard quasi-static tensile tests were carried out in a 1200 kN tensile testing machine with displacement control at the constant strain rate of $4 \times 10^{-5}\,s^{-1}$. The specimens were laser cut in rolling direction to the desirable geometry as shown in Fig. 2(a).

The specimens were laser cut from the middle prior to joining process and the cut edges were machined sufficiently. The machining assures that no effect from laser cutting remains prior to the welding process. The laser cut edges of the specimens (as highlighted in red colour in Fig. 2(a)) were also machined to remove any effect of heat generated from laser cutting. For the GMAWs, a 60° double-V groove shape with air gap of 1 mm was prepared as shown in Fig. 2(b). However, the specimens for laser welding were machined in a straight 90° angle with a zero air gap forming a keyhole shape weldment.

In order to obtain detailed information about the local behaviour of the weldments, especially at the HAZ during tensile testing, a 3D optical measurement device (ARAMIS) was utilized. To generate the full field measurement images, a random pattern is required which can be created via black dots on a white painted surface. Prior to tensile testing, the specimens were kept in a 6% nitric acid solution for 24 h so that the paint adhered well to the surface during testing. The spray-painting of the specimens were done after acid cleaning and right before performing each test.

3.2. Welding process

In the current study, three steel grades including S700, S960 and S1100 were butt-welded (BW). In order to weld the plates, two processes were considered including GMAW, and LW. Both of the welding processes were performed using a robotized system in order to attain high quality welding consistently. For the GMAW, double V-groove

Table 1
The nominal chemical composition of the BMs (wt. %).

Steel	C	Si	Mn	P	S	V	Cu	Cr	Ni	Mo	CEV
S700	0.12	0.25	2.10	0.020	0.10	0.20	–	–	–	–	0.38
S960	0.088	0.04	1.13	0.010	0.000	0.009	0.011	1.00	0.05	0.117	0.59
S1100	0.133	0.192	1.49	0.006	0.001	0.152	0.437	1.34	0.998	0.388	0.85

Table 2
The nominal mechanical properties of virgin plates.

Steel	Yield strength (min) [MPa]	Tensile strength [MPa]	A_5 (%)
S700	700	750–950	13
S960	1052	1116	10
S1100	1167	1199	14.5

Table 3
Nominal chemical compositions and mechanical properties of filler materials (wt. %).

Filler material	C	Si	Mn	Cr	Mo	Ni
Union Ni 2.5	0.08	0.60	1.00	–	–	2.35
Union X96	0.12	0.80	1.90	0.45	0.55	2.35

	Yield strength	Tensile strength	Elongation	Impact strength	
	f_y [MPa]	f_u [MPa]	A_5 [%]	T [°C]	KV [J]
Union Ni 2.5	510	620	24	−70	47
Union X96	930	980	14	−50	47

shapes with two different welding speeds were considered: 3.1 and 6.2 mm/s, which stand for high and low HI, labelled as HQ and LQ, respectively. The HQ specimen stands for approximate heat input value of 1.4 kJ/mm for each weld pass, calculated according to [32]:

$$Q = \varepsilon \times U \times I/(v \times 1000) \quad (kJ/mm) \tag{1}$$

where ε is the thermal efficiency of the welding procedure which is 0.8 for the GMAW. U, I and v are the welding arc voltage, current and moving head speed.

The welding speed of HQ specimens is in the range of hand welding so that it is comparable with an in site welding [33]. Cooling rate ($t_{8/5}$) is calculated according to [34]:

$$t_{8/5} = (4300 - 4.3T_o) \times 105 \times \frac{Q^2}{d^2} \times \left[\left(\frac{1}{500 - T_o}\right)^2 - \left(\frac{1}{500 - T_o}\right)^2\right] \times F_2 \tag{2}$$

where T_o is the preheat or ambient temperature (assumed as 20 °C for this test), Q is the welding heat input, d is the plate thickness, and F_2 is the shape factor for the two-dimensional heat flow (0.9 for butt welds).

The LQ specimens have heat input of 0.7 kJ/mm for each welding pass, which is below 1 kJ/mm recommended in the literature [20]. The LQ specimens have a rather fast cooling rate with $t_{8/5}$ of 8 s. The welding filler materials were in match condition for each steel grade. The

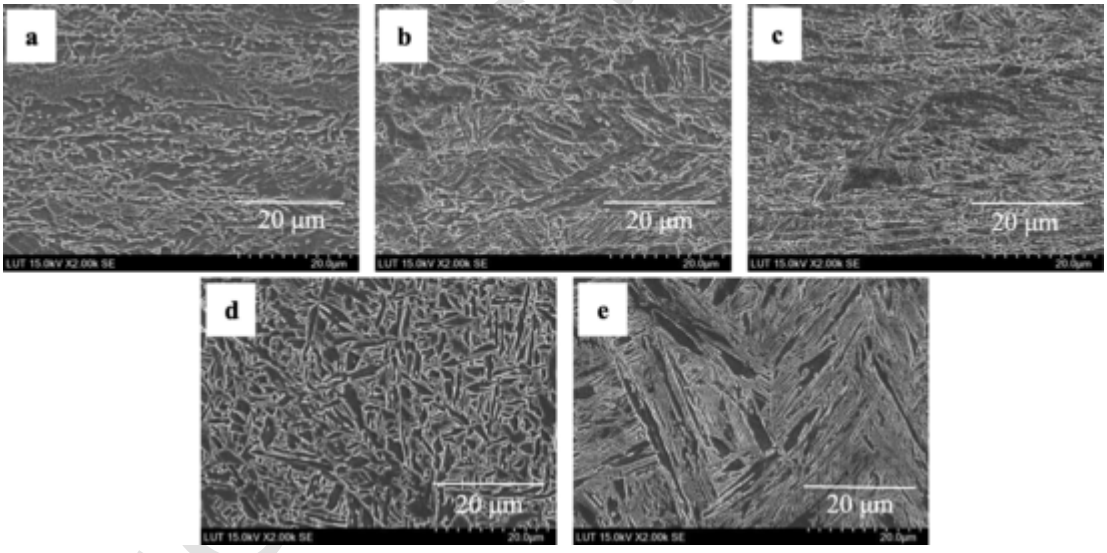

Fig. 1. SEM micrographs of: (a) S700, (b) S960, (c) S1100, (d) Union Ni 2.5, and (e) Union X96.

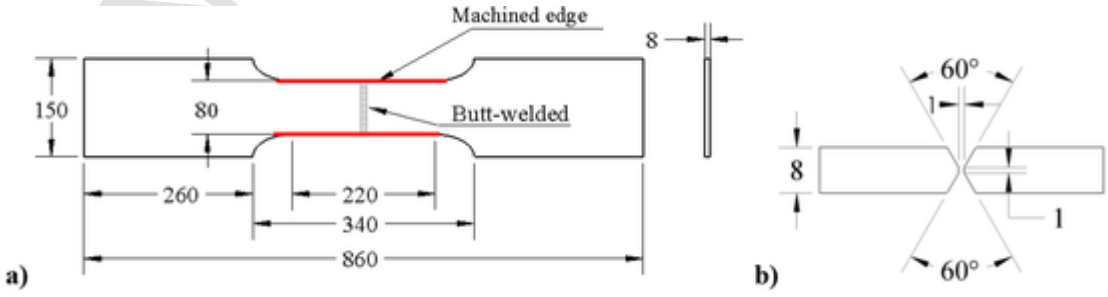

Fig. 2. (a) The geometry of welded specimen and (b) double-V groove shape for GMAW. (Dimension in mm, not to scale).

welding torch was in 5° angle towards the pushing direction. The applied welding parameters are shown in Table 4.

For the LW, a 10 kW fibre laser machine with mounted a Precitec YW50 optical head was utilized. The laser beam was then focused using a 300 mm lens and collimation of 150 mm resulting a round spot shape with radius of 0.2 mm. The laser beam was focused 3 mm below the surface of the specimen creating a keyhole shape. No filler material was used for the LW specimens which results in a perfect match welding. The laser beam was passing on the surface of the weldment with speed of 30 mm/s which is considered as a very fast welding process. The applied welding parameters are listed in Table 4. Note that the cooling rate for LW specimens is calculated according to [19]. The very fast LW resulted in $t_{8/5}$ of 0.8 s, which is considered as a very fast cooling rate.

3.3. Microhardness measurements

The cross-section of the specimens was polished in order to closely examine through thickness of the weldments and measure Vickers micro hardness values across the weld. Accordingly, surface grinding using abrasive particles was performed for 4 min with particles having roughness of 120 μm. Fine grinding was then applied for 4 min using diamond particles with roughness of 9 μm. The specimens were then undergone final polishing for 6 min using diamond particles with roughness of 3 μm. Afterwards, the specimens were etched with Nital 5% for 15 sec. Fig. 3 shows polished sections of the weldments.

Micro-indentation hardness of the polished sections after welding was measured in different zones, using a Vickers micro-hardness machine (Durascan 70). The applied load and dwell period were, respectively, 5 kgf and 10 sec. Measured points were collected along three horizontal lines including 1 mm below the surface (top line), the middle of the weldment (middle line), and 1 mm above the bottom of cross-section (bottom line). For the GMAW specimens (HQ and LQ), the top and bottom lines represent the second and first weld passes, respectively.

4. Results and discussion

4.1. Tensile behavior of the weldments

In order to study the mechanical properties of weldments made of HSS/UHSS, the specimens were tensile tested at ambient temperature and load-displacement curves are compared as shown in Fig. 4. The tensile characteristics of the butt-welded joints such as Young's modulus (E), yield and ultimate strength (f_y and f_u, respectively), strain at yield and ultimate strength (ε_y and ε_u, respectively), elongation at rupture point (A) were then extracted from the ARAMIS software accordingly. The aforementioned mechanical properties of each weldment are presented in Table 5, which are governed from the engineering stress-strain curves. Besides, in order to better understand the distribution of strains at the specimens, the 3D full field measurement images were compared. Fig. 5 shows the last captured image right before failure happening at the specimens.

When the BMs of the three steels are compared (S700, S960 & S1100), the S700 and S1100 show similar elongation at break which is 12.9% and 11.8%, respectively. It is notable that these two steels undergo a similar Q&T process during their manufacturing procedure. However, the S960 which is a DQ type of steel shows 7.5% of elongation at its rupture point. When f_u/f_y is compared, the S960 shows the highest value which is 1.16, compared to 1.11 and 1.05 for S700 and

Table 4
The applied welding parameters.

GMAW									
		Weld	Filler	I	U	Wire feed	v	Q [32]	$t_{8/5}$ [34]
		[No.]	material	[A]	[V]	[m/min]	[mm/s]	[kJ/mm]	[s]
S700	HQ	1	Union Ni 2.5	221	25.0	10.0	3.1	1.43	33
		2		216	25.1	10.0	3.1	1.40	31
	LQ	1	Union Ni 2.5	219	25.1	10.0	6.2	0.71	8
		2		219	25.1	10.0	6.2	0.71	8
S960	HQ	1	Union X96	225	25.0	10.0	3.1	1.45	34
		2		220	25.1	10.0	3.1	1.43	33
	LQ	1	Union X96	214	25.1	10.0	6.2	0.69	8
		2		217	25.1	10.0	6.2	0.70	8
S1100	HQ	1	Union X96	222	25.1	10.0	3.1	1.44	33
		2		210	25.1	10.0	3.1	1.36	30
	LQ	1	Union X96	217	25.1	10.0	6.2	0.70	8
		2		223	25.1	10.0	6.2	0.72	8

LW					
	Power	F	v	Q	$t_{8/5}$ [19]
	[kW]	[mm]	[mm/s]	[kJ/mm]	[s]
S700 S960 S1100	9	−3	30	0.3	0.8

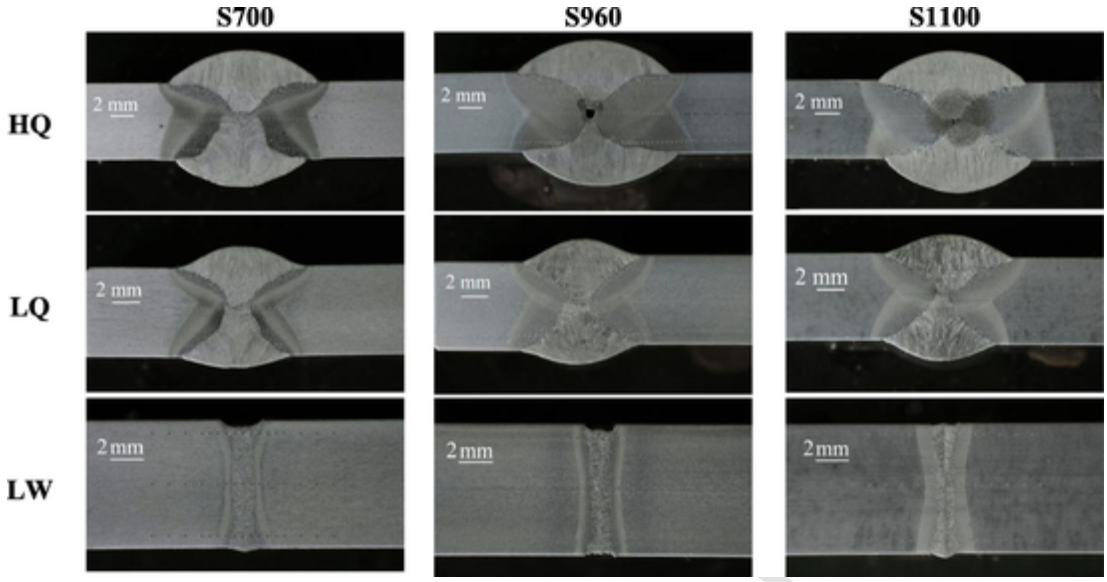

Fig. 3. Polished sections of the weldments.

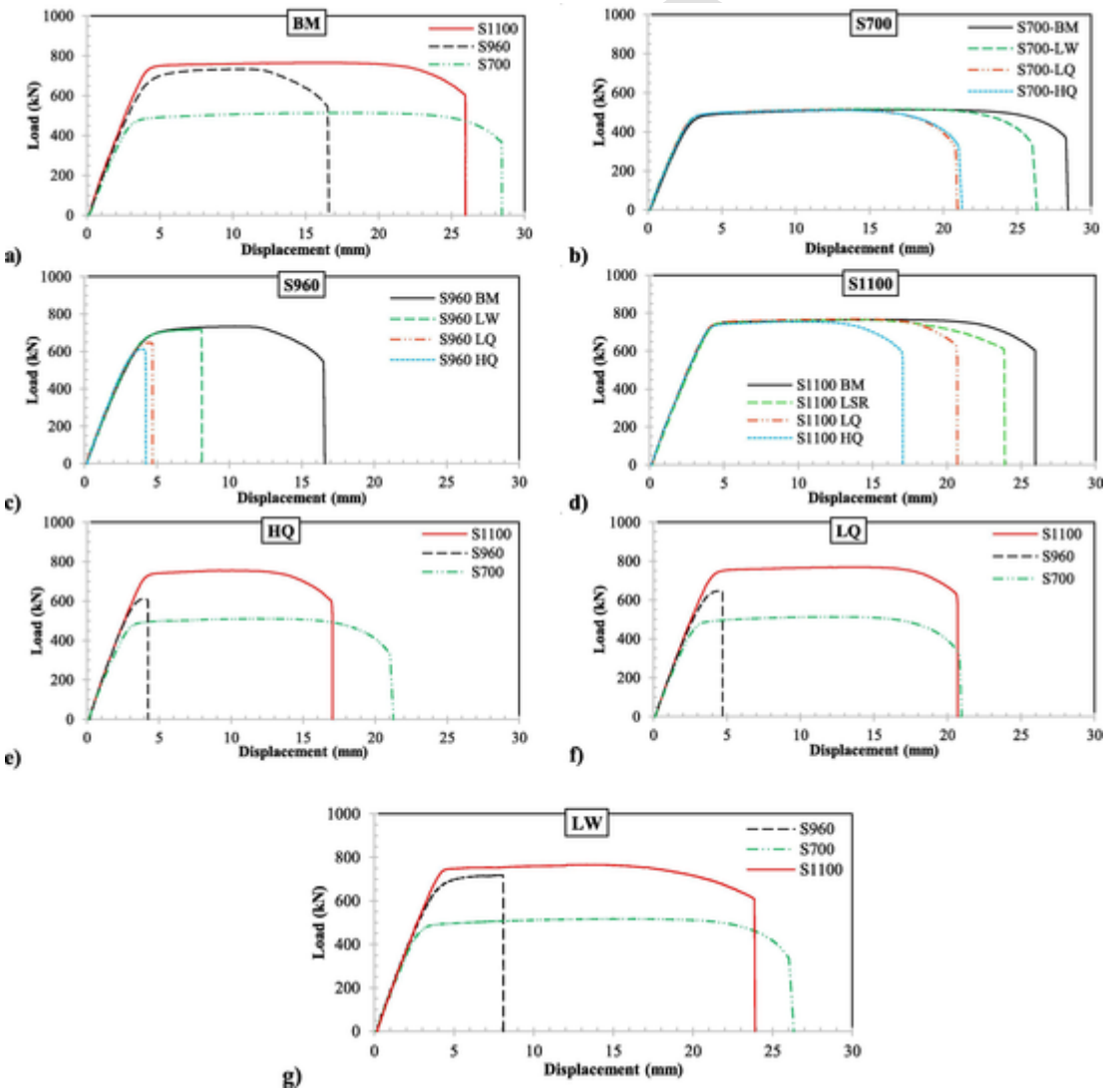

Fig. 4. Tensile test results: (a) BMs, (b) S700, (c) S960, (d) S1100, (e) high HI, (f) low HI and (g) LW.

Table 5
The mechanical properties of weldments compared with BM.

Steel Grade		E [GPa]	f_y [MPa]	ε_y (%)	f_u [MPa]	ε_u (%)	A [%]	(f_u/f_y)	$\varepsilon_u/\varepsilon_y$
S700	BM	194	723	0.53	801	6.30	12.9	1.11	11.98
	LW	199	741	0.47	806	5.61	11.8	1.09	11.93
	LQ	194	725	0.51	785	4.76	9.5	1.08	9.43
	HQ	195	747	0.46	803	4.02	9.6	1.07	8.71
S960	BM	204	989	0.62	1152	2.65	7.5	1.16	4.27
	LW	203	976	0.59	1097	2.39	3.1	1.12	4.05
	LQ	198	922	0.61	1008	1.12	1.8	1.09	1.84
	HQ	193	864	0.60	915	0.93	1.5	1.05	1.54
S1100	BM	209	1174	0.72	1235	6.63	11.8	1.05	9.20
	LW	205	1133	0.70	1171	4.39	11.3	1.03	6.27
	LQ	213	1127	0.71	1187	4.36	9.4	1.05	6.14
	HQ	213	1124	0.69	1170	3.17	7.7	1.04	4.59

S1100, respectively. However, when $\varepsilon_u/\varepsilon_y$ is compared, S700 has the highest value which is 11.98. The S960 and S1100 have $\varepsilon_u/\varepsilon_y$ values of 4.27 and 9.20, respectively. According to [18,29,30], ductility of UHSS decreases by increasing the steel' grade; However, the studied S1100 shows a higher ductility compared to S960. Accordingly, f_u/f_y is not the only parameter that should be used in order to govern ductility of HSS/UHSS. Other parameters such as $\varepsilon_u/\varepsilon_y$ and plastic strain capacity of the steel up to the rupture should also be considered.

The S700 shows almost no reduction in its yield and ultimate strength when butt-welds are manufactured using various HIs. Fig. 5 also demonstrates that the plastic strains are concentrated at the BMs of all S700 specimens followed by 30° angle of the fracture plane. Inclined angle of fracture as the result of localization of shear bands is reported in literature by Anand and Spitzig [35], who proposes 45° angle of the fracture plane. However, for higher grades of steel, the fracture angle seems to form at 30° [3,36]. Björk et al. [37] demonstrate that consideration of the critical plane based on simple force balance and von Mises yield criterion approach will give a 30° angle of fracture. The average f_y and f_u of the material is calculated as 734 and 799 MPa, respectively with a 2% of variation. However, when ductility of the weldments made of S700 is compared, the LW specimen shows the best performance reaching over 90% of the BM's elongation. The LQ and HQ specimens show greater reduction in elongation by reaching 74% of the BM's capacity. As can be seen from Fig. 5, the distribution of plastic strains at BM and LW specimens are much homogeneous compared to the specimens welded via GMAW. The weld reinforcement of the LQ and HQ specimens act as a constraint preventing the plastic flow to spread homogeneously across the gauge area reducing plastic strain capacity of weldments. According to the tensile test results, there is no major changes in the load level at which failure has happened when the welded specimens of S700 are compared to the BM. It is evident that increasing the welding HI reduces ε_u, A, f_u/f_y, and $\varepsilon_u/\varepsilon_y$ of the weldments. The ductility reduction is also reported by Liu et al. [38], when the mechanical properties of a similar HSS (S690-QT) was studied with HI varying from 1.0 to 5.0 kJ/mm. It should be pointed out that cylindrical coupons of the welded sections were used in [38] rather than the flat "dogbone" type of specimen used in this paper (see Fig. 2). The reduced yield strength for the welded sections with HI of 1.0, 1.5, 2.0 and 5.0 kJ/mm were 0.98, 0.90, 0.86 and 0.70 of that of the base plates respectively [38]. Similarly, the reduced tensile strength for the welded sections with HI of 1.0, 1.5, 2.0 and 5.0 kJ/mm were 0.998, 0.97, 0.92 and 0.83 of those of the base plates, respectively [38]. The HI of 1.0 is slightly higher than that of LQ (0.7 kJ/mm), whereas HI of 1.5 is slightly higher than that of HQ (1.5 kJ/mm) used in this paper.

It is notable that no weld porosity was found when GMAW is applied to the butt-joint S700 steel plates, regardless of the value of HI introduced to the material up to 1.4 kJ/mm for each welding pass. The S700 LW specimen shows 0.5 mm porosity in the form of concavity at the upper surface of the weldment, which appears to have no effect on the joint's capacity.

The S960 shows considerable reduction in f_y and f_u followed by a greater decrease in its ductility after welding. The magnitude of f_y changes from 989 to 864 MPa which is equivalent to 13% of reduction when welded using the highest HI compared to the virgin plate. Moreover, f_u of the joint shows 21% of capacity reduction falling from 1152 to 915 MPa when 1.4 kJ/mm of HI is applied to weld the material. The experiments show that f_u/f_y also reduces from 1.16 to 1.05 when the steel plate is welded via GMAW. It is also notable that for all of the welded specimens of S960, failure has happened at a higher loading compared to the BM. Yet the major concern is the reduction in the ultimate elongation of the S960 weldment, which falls from 7.5% to 1.5% after welding with the highest HI. Table 5 shows that welding HI has a considerable effect on the reduction of ε_u, A, f_u/f_y, and $\varepsilon_u/\varepsilon_y$. The weldment prepared via LW shows the best performance reaching the BM's f_y and f_u. However, still over 50% reduction in ductility of the LW is notified. Farrokhi et al. [19] reported that by increasing the laser power to 9.5 kW, and the welding speed to 47 mm/s, it is possible to reach higher cooling rates and a narrower HAZ, eventually reaching BM's elongation capacity. To accomplish this, a special laser head system is required which was out of the capability of the current research. As can be seen from Fig. 5, while the welded specimen of S960 is still experiencing loads at the elastic region, the HAZ undergoes plastic deformations. The concentrated plastic strains at the HAZ leads to failure at zero degree angle of the fracture plane. The LW specimen shows that the plastic strains are forming at the 30° fracture angle, however, a crack initiates at the HAZ leading failure at this zone.

A closer look at the polished cross-section of the weldments of S960 shows that increasing the welding HI also increases the chance of weld porosity as shown in Fig. 3. A major porosity is notable at the middle of HQ specimen which can affect the static capacity of the joint. Even though the weld root was opened after the first weld pass to make sure there is no lack of penetration, yet formation of porosity was negligible when high HI is applied. Besides, the LW specimen also shows 0.5 mm weld porosity in the form of concavity at the top surface and a minor welding instability at the bottom.

As can be seen from Fig. 5, the S1100 specimens have failed at the BM outside welded region at the 30° fracture plane. Table 5 also demonstrates that the effect of HI on f_y and f_u is negligible for this steel grade. The average values for f_y and f_u are 1140 and 1197 MPa, respectively, with 3% of variation. The difference in the measured f_y and f_u is

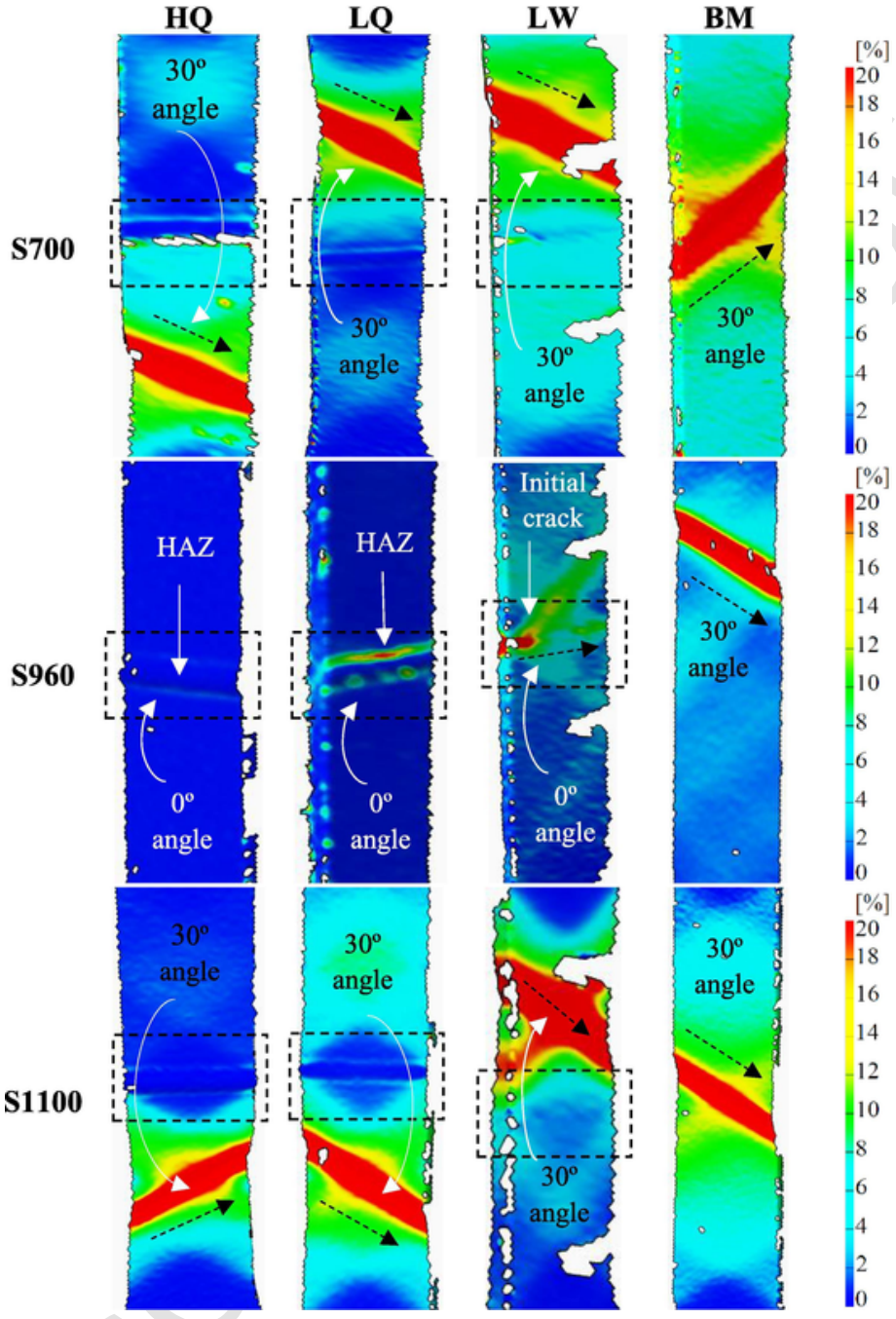

Fig. 5. 3D optical measurements showing distribution of strains across the specimens at the time of failure (welded area is highlighted via dashed box).

possibly due to the random micro-defects in the manufactured material. However, all the welded specimens satisfactorily passed the minimum yield and ultimate strength criteria. The f_u/f_y value for this steel grade remains almost intact regardless of the welding method and the magnitude of HI. However, ductility of the welded joints is prone to be sensitive to welding HI energy, especially for HI values over 1 kJ/mm. It is notable from Table 5 that welding HI has reduced ε_u, which consequently reduced the magnitude of $\varepsilon_u/\varepsilon_y$. Fig. 5 also demonstrates the constraint effect by the weld reinforcement which has reduced ductility of the joint. The HQ specimen specially shows that bigger weld reinforcement affects ductility of the joint more. The flow of strain at the LW specimen is distributed homogeneously letting the whole gauge area undergo plastic region, eventually reaching ductility of the BM. No significant change in the failure loads of welded S1100 specimens comparing to the BM is observed.

The appearance of weld porosity at the S1100 HQ specimen is also notable which is due to excessive HI. The weld porosity has not affected the static yield and ultimate strength of the material. However, it can greatly affect the fatigue life of the weldment. As can be seen from Fig. 3, the LW S1100 specimen shows no weld defect or instability during welding process resulting the best weld quality compared to LW specimens made of S700 and S960.

4.2. Micro-hardness analysis

Fig. 6 shows distribution of hardness values across the weldments of all specimens in which a drop in the magnitude of hardness values at

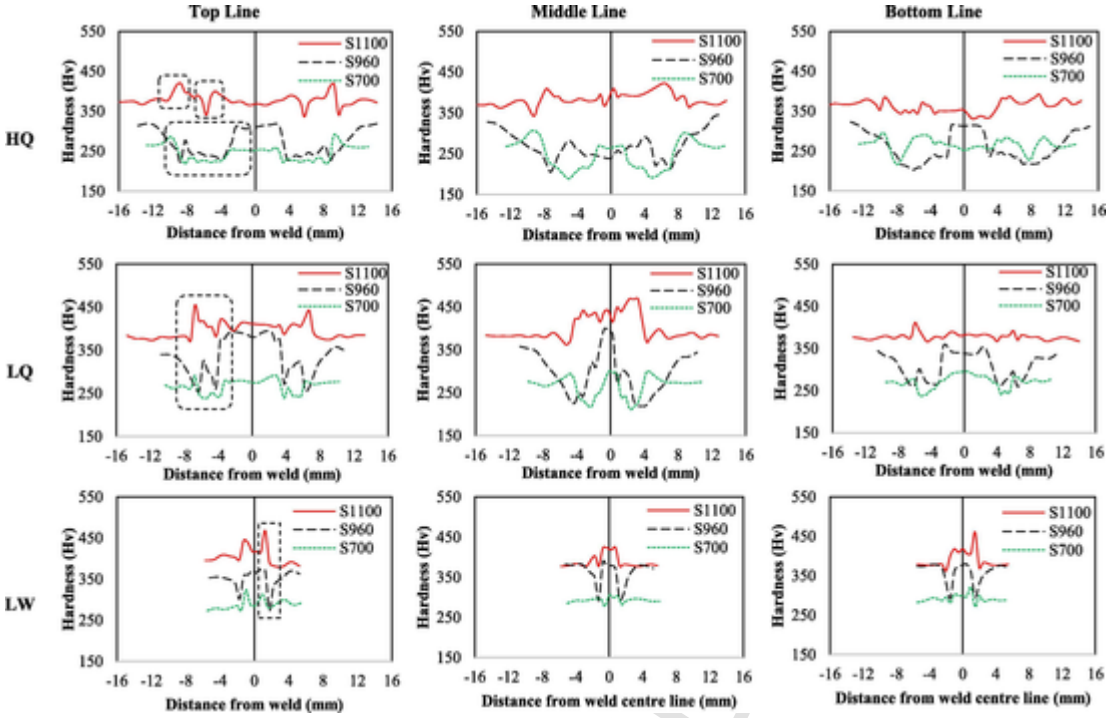

Fig. 6. Hardness distribution at the weldments.

the softened HAZ is visible. The HAZ at the top line is highlighted with a dotted box. Table 6 shows the minimum hardness values at the softened HAZ. According to the results, S960 shows the highest reduction when compared to other steels welded with similar HI. The highest reduction corresponds to S960 HQ, which is 46%, followed by 34% and 11% when HQ specimens were made from S700 and S1100 steels, respectively. A similar behavior is also seen when LQ specimens are compared, i.e. S960 is showing 41% of reduction in the magnitude of hardness, the S700 and S1100 show 26% and 4% reduction, respectively. The LW specimens reveal a slight difference since S700 and S1100 have similar performance with hardness reduction only in the range of 4–6%. However, the LW specimen made of S960 still shows considerable 21% of reduction in the magnitude of hardness.

All in all, the S1100 steel material tends to have the highest resistance to HI and the minimum reduction in the hardness values. The higher resistance to HI is referred to the less degradation of the steel' hardness. This is in contrast with the available results from similar steel grades presented in the literature [21–23,29,30] in which they observed reduction in the hardness values by increasing the steel's grade after welding. Some explanations will be given in Section 4.3.

It is also notable that the area of HAZ has different sizes for the three steels. The S1100 has the smallest among the studied steel followed by S700 and S960, respectively. According to Amraei et al. [20] when the HAZ is very small, the surrounding BM, both in the through-thickness and on the surface, creates a strong boundary condition and, thus, a hydrostatic stress component develops in transverse and through-thickness directions. The hydrostatic stress component increases the magnitude of the stress required in the loading direction to reach the yield point in the HAZ. In other word, a higher stress in the loading direction is required to yield the HAZ.

Moreover, the correlation between micro-hardness values and mechanical properties were proposed by Murakami [39], and Pavlina & Van Tyne [40]. According to Murakami [39],

Table 6
Correlation between hardness values and mechanical properties of the weldments.

Steel	Zone	Hardness		f_y			f_u				
		Measured (Hv)	Reduction (%)	Measured f_y (MPa)	P&V (MPa)	D (P&V/f)	Measured f_u (MPa)	M_{min} (MPa)	M_{max} (MPa)	P&V (MPa)	D (P&V/f_u)
S700	BM	287	–	723	735	1.02	801	861	976	972	1.21
	LW	271	6	741	689	0.93	806	813	921	912	1.13
	LQ	212	26	725	519	0.72	785	636	721	692	0.88
	HQ	188	34	747	450	0.60	803	564	639	602	0.75
S960	BM	374	–	989	985	1.00	1152	1122	1272	1297	1.13
	LW	274	27	976	697	0.71	1097	822	932	923	0.84
	LQ	221	41	922	545	0.59	1008	663	751	725	0.72
	HQ	203	46	864	493	0.57	915	609	690	658	0.72
S1100	BM	378	–	1174	996	0.85	1235	1134	1285	1312	1.06
	LW	362	4	1133	950	0.84	1171	1086	1231	1252	1.07
	LQ	362	4	1122	950	0.85	1187	1086	1231	1252	1.05
	HQ	336	11	1124	876	0.78	1170	1008	1142	1155	0.99

$$0.5f_u = 1.6Hv \pm 0.1Hv \quad (3)$$

where Hv is the Vickers hardness, and f_u is the ultimate strength of the material. This equation does not provide a correlation between yield strength and Vickers hardness of steel.

However, according to Pavlina & Van Tyne [40], it is possible to correlate Hv to f_y and f_u for the steels with yield strength between 300 and 1700 MPa as such:

$$f_y = -90.7 + (2.876Hv) \quad (4)$$

and,

$$f_u = -99.8 + (3.734Hv) \quad (5)$$

The yield and ultimate strengths were calculated according to Eqs. (3)–(5) as shown in Table 6 where "M" stands for the ultimate strength calculation according to Eq. (3), "P&V" stands for the calculations according to Eqs. (4) and (5). The deviation between calculated values according to Eqs. (3) and (4) and measured experimental values are shown as "D". Since Eq. (3) only shows a range, M_{max} and M_{min} are introduced.

Eq. (4) successfully predicts the yield strength of both S700 and S960; however, it has 15% error to calculate the yield strength of S1100. This error is still within the prediction range by [40] since −200 to +50 MPa of variation for the hardness values between 300 and 400 Hv is considered. It is also notable that the S1100 studied in this paper has a complex microstructure with a mixture of bainite, martensite and retained austenite in which only seven quite scattered data points with similar microstructure were available in Pavlina & Van Tyne's study [40].

When the minimum hardness values are considered to predict the yield strength of the weldment, Eq. (4) fails to accurately predict the correlation between yield strength and hardness of the HAZ. This could be due to the boundary condition effect of the neighboring material as explained above. With increasing the HI where hardness values drop to lower values, the predictions become even more inaccurate.

Eq. (3) fairly predicts the range of ultimate strength of the BMs. It also provides a range in which weldments of S1100 can fit within; however, there is considerable 200 MPa range. Eq. (5) also fairly predicts the ultimate strength of S1100 weldments since they have the minimum reduction in the hardness values. All in all, the above equations cannot accurately estimate the mechanical properties of the weldments made of HSS/UHSS. Further experimental tests are required to find a better correlation between hardness values and strength of welded HSS/UHSS.

4.3. Microstructure analysis

The microstructural features of welded specimens are analyzed using SEM. In order to study the effect of HI on the microstructure of each weldment, four zones were considered including: the BM, softened HAZ after two heat passes, HAZ after one heat pass and the weld fusion zone.

Figs. 7–9 show the microstructure of welded S700 at different zones. The BM of S700 consists of a mixture of bainite, islands of martensite-austenite (M/A), and small blocks of retained austenite along the high-angle grain boundaries [41]. After welding, the softened HAZ shows a mixture of tempered martensite and granular bainite [42]. The hardness drop is due to the existence of granular bainite, since this feature is naturally softer than bainite and martensite [12,43]. Due to the higher cooling rate, the LW specimen shows a finer texture of bainite and M/A at its softened HAZ compared to the GMAW specimens, which resulted in less hardness drop. The very large microstructural features at the softened HAZ of HQ specimen resulted

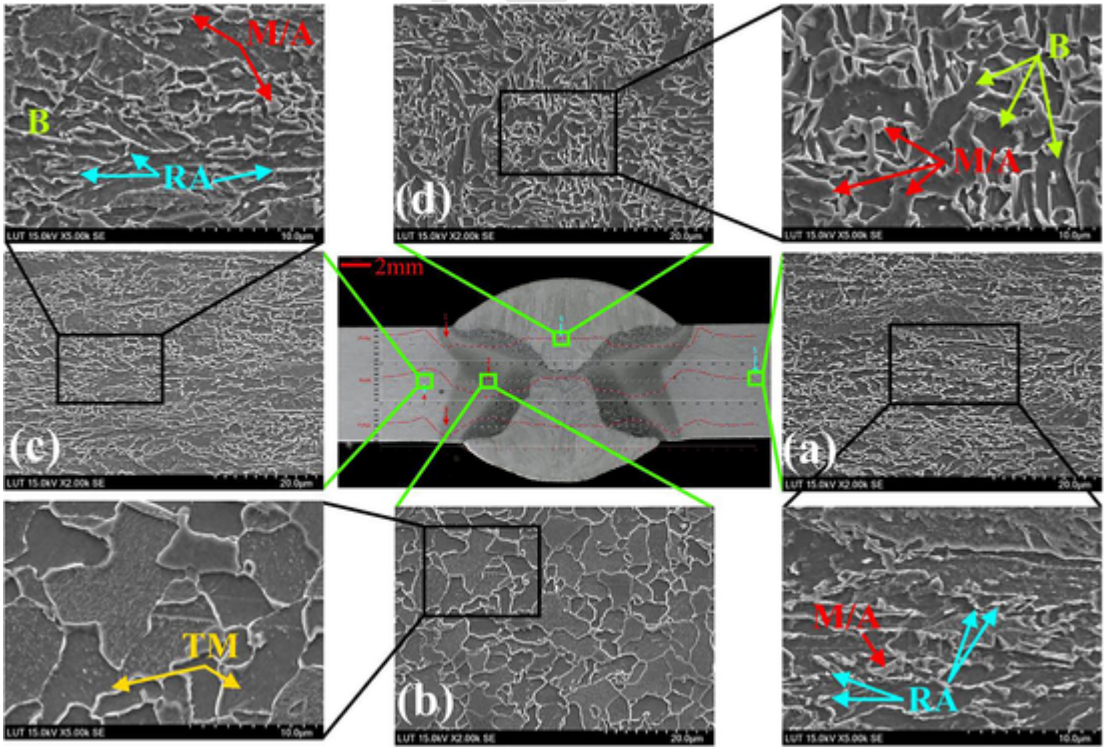

Fig. 7. SEM micrographs of S700-HQ at: (a) BM (M/A: martensite-austenite islands, RA: retained austenite, background is bainite), (b) softened HAZ (TM: tempered martensite, background is granular bainite), (c) HAZ (B: bainite as the background microstructure), and (d) weld filler material.

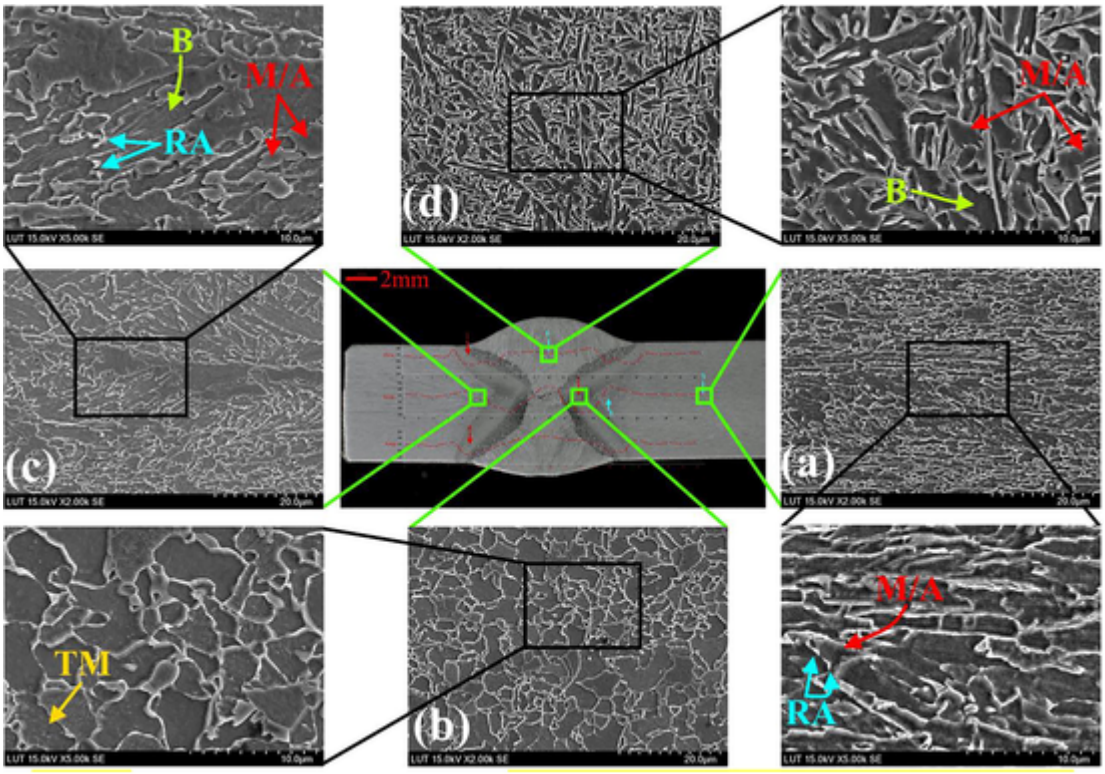

Fig. 8. SEM micrographs of S700-LQ at: (a) BM (M/A: martensite-austenite islands, RA: retained austenite, background is bainite), (b) softened HAZ (TM: tempered martensite, background is granular bainite), (c) HAZ (B: bainite as the background microstructure), and (d) weld filler material.

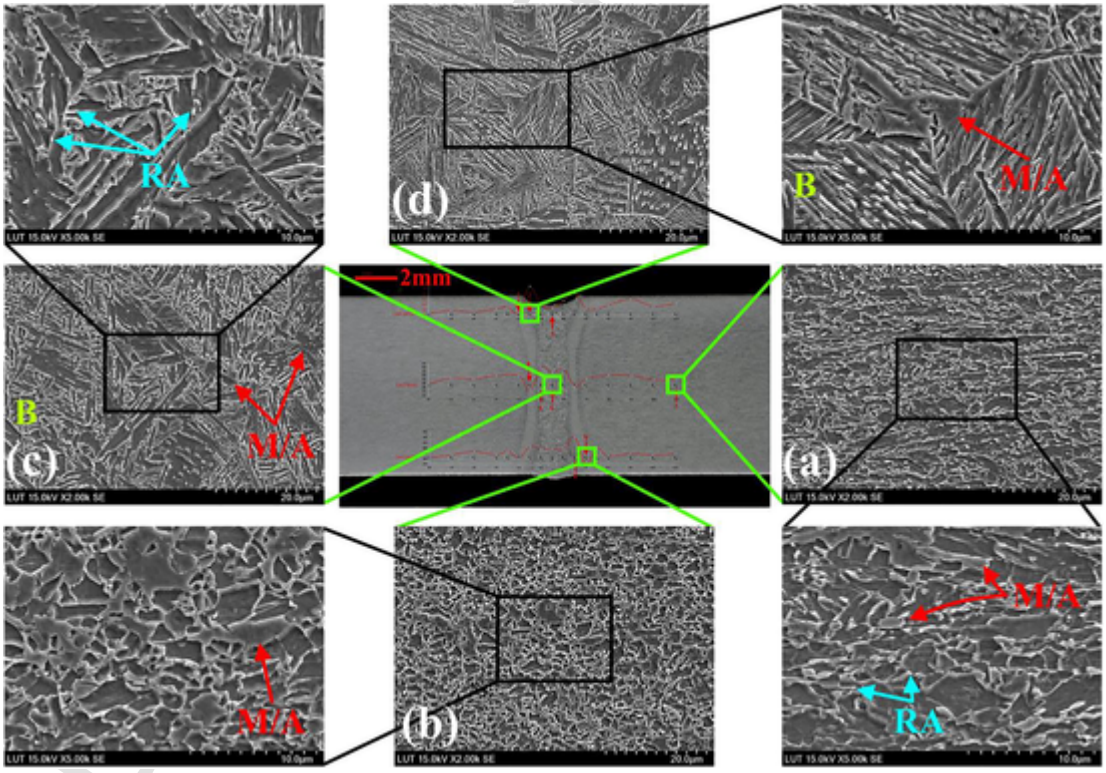

Fig. 9. SEM micrographs of S700-LW at: (a) BM (M/A: martensite-austenite islands, RA: retained austenite, background is bainite), (b) softened HAZ (Background is bainite), (c) weld area (B: bainite as the background microstructure), and (d) weld fusion line.

in the most severe hardness drop. No significant difference between the microstructural features after the second welding pass is notable.

As can be seen from Figs. 7 and 8, the filler materials of HQ and LQ specimens have a mixture of bainite and M/A as their microstructure. However, larger microstructural features due to the higher HI are notable for the HQ specimen. Fig. 9 shows that the fusion zone of the LW specimen is a fine textured combination of bainite, islands of M/A, and some retained austenite which is similar to the BM. However, the microstructural features are finer, compared to the BM due to very high cooling rate of the laser welding.

Figs. 10–12 show the microstructure of welded S960 at different zones. According to Figs. 10(a) and 11(a), the BM of S960 consists of bainite, islands of M/A, tempered martensite, and retained austenite. The welding HI seems to have a major impact on the microstructural features at the softened HAZ of S960. That is the reason why welded S960 specimens show various levels of hardness reduction. Moreover, by comparing Figs. 10(b) with (c) and 11(b) with (c), it is notified that microstructural features change in multi-pass welding for this steel. According to these figures, the softened HAZ of HQ specimen after the second weld pass consists of a mixture of granular bainite and bainite. The softened HAZ after the first weld pass is influenced by the reheating and cooling by the second weld pass. Even though this area is also composed of a mixture of granular bainite and bainite, they are transformed from larger prior austenite grains. Thus, in comparison to the second pass, the granular bainite consists of larger polygons of ferrite accompanied by a higher portion of larger M/A islands. Thus, reheating results in the larger prior austenite grains (consequently a larger texture for granular bainite), and a decrease in bainite content in the area, which ultimately results in more hardness drop for the HAZ of the first weld pass.

As can be seen from Fig. 11(c), the softened HAZ of LQ specimen after the second weld pass consists of granular bainite and bainite, similar to HQ sample. However, the texture is finer compared to HQ specimen due to the lower HI (and higher cooling rate) during the welding process. The reheating process of the LQ specimen also resulted in larger prior austenite grains. However, due to its higher cooling rate compared to the HQ specimen, the softened HAZ only consists of bainite, M/A, and some tempered martensite with no evidence of granular bainite. Due to the very high cooling rate of laser welding, the softened HAZ of the LW specimen is a fine textured mixture of bainite and M/A. These microstructural features resulted in a moderate hardness drop in the LW specimen, compared to HQ and LQ.

As can be seen from Figs. 10(d) and 11(d), the fusion zones of specimens welded with GMAW are a mixture of bainite and M/A. Due to the high cooling rate of laser welding, the LW specimen, welded without the addition of any filler material, is also a mixture of bainite and M/A at its fusion zone.

Figs. 13–15 show the microstructure of welded S1100 at different zones. The BM is a mixture of bainite, islands of M/A, and small islands of retained austenite scattered along the high-angle grain boundaries [12]. Similar to the microstructure of the BM, the softened HAZ of all welded specimens are a combination of bainite, M/A, and retained austenite, regardless of their welding process. The similarity in the microstructural features of welded S1100 specimens resulted in much lower hardness drop compared to S700 and S960. However, S1100-HQ showed that by increasing the HI values, size of the microstructural features increased too, which resulted in more hardness reduction comparing to LQ and LW specimens. As can be seen from Fig. 6, the hardness distribution graphs show a peak in the magnitude of hardness next to the softened HAZ. According to Figs. 13(c) and 14(c), these areas are fine textured mixture of bainite and M/A, as the products of normalized austenite fast cooling. The higher hardness values at these regions can be attributed to the smaller size of their microstructural features which seemed to be the result of normalization and thermal gradient they have experienced through the welding, based on their distance from the fusion line. No significant difference between the microstructural features after the second welding pass is notable.

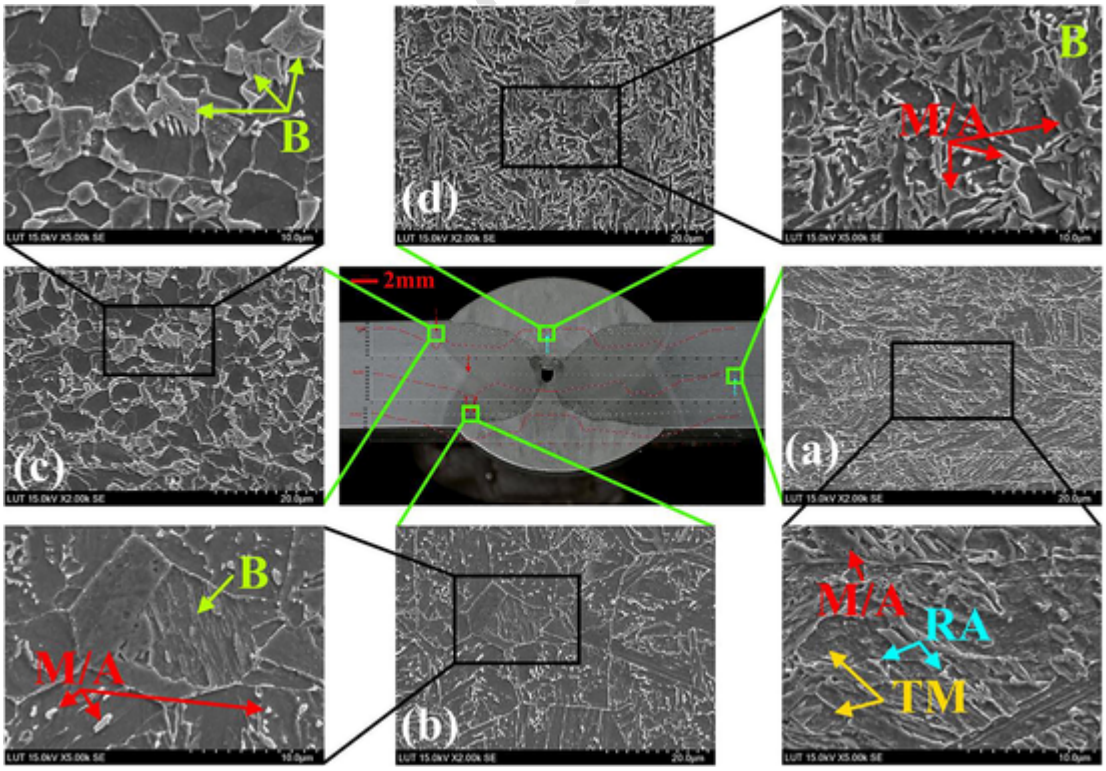

Fig. 10. SEM micrographs of S960-HQ at: (a) BM (M/A: martensite-austenite islands, TM: tempered martensite, RA: retained austenite, background is bainite), (b) softened HAZ after the first weld pass (B: bainite, background is coarse-grained granular bainite), (c) softened HAZ after the second weld pass (background is granular bainite), and (d) weld filler material (B: bainite as the background microstructure).

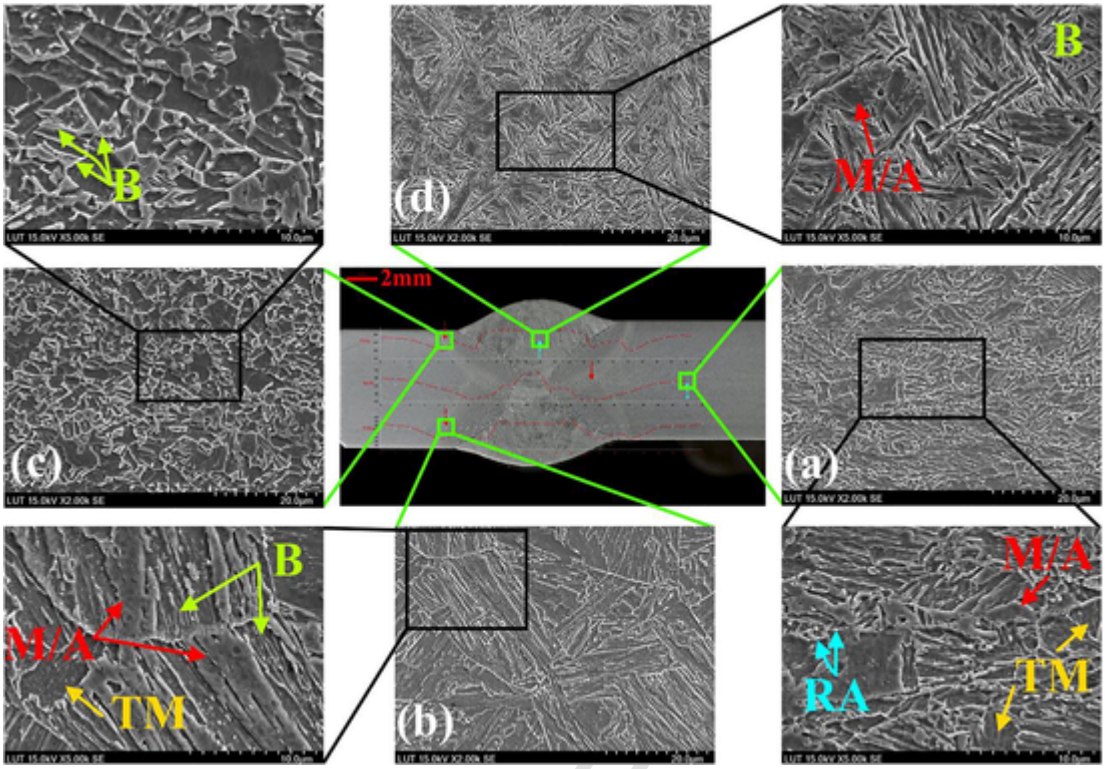

Fig. 11. SEM micrographs of S960-LQ at: (a) BM (M/A: martensite-austenite islands, TM: tempered martensite, RA: retained austenite, background is bainite), (b) softened HAZ after the first weld pass (B: bainite), (c) softened HAZ after the second weld pass (background is granular bainite), and (d) weld filler material (B: bainite as the background phase).

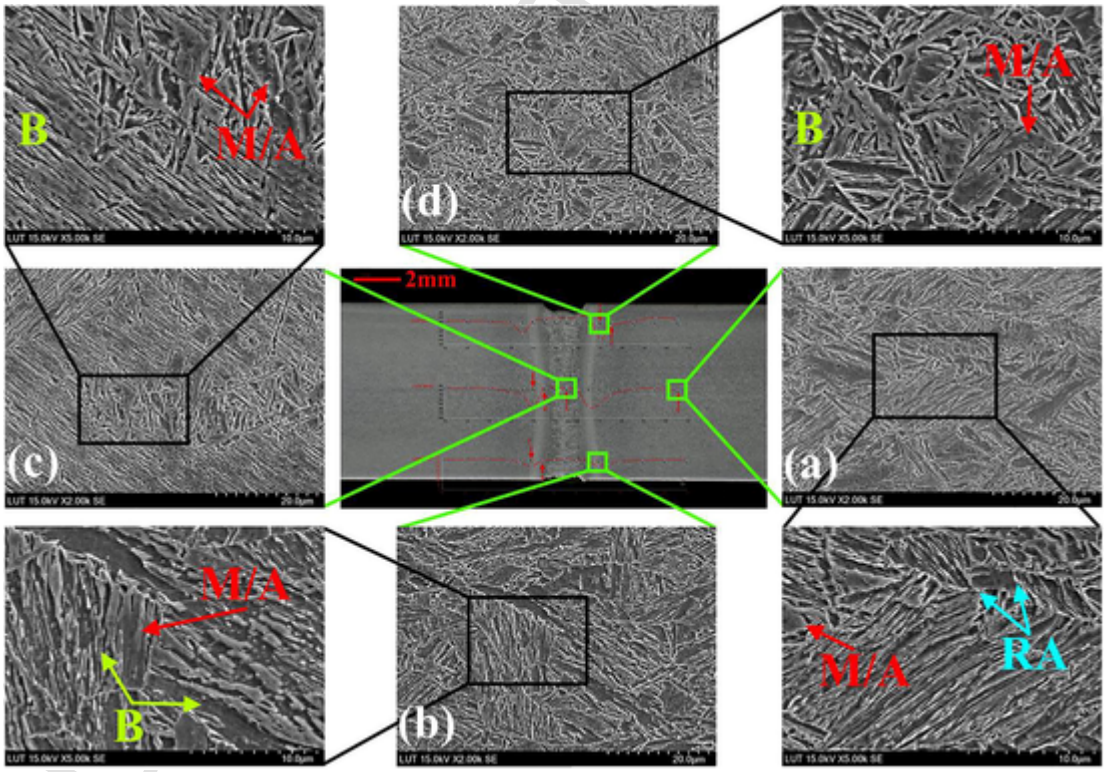

Fig. 12. SEM micrographs of S960-LW at: (a) BM (M/A: martensite-austenite islands, RA: retained austenite, background is bainite), (b) softened HAZ (B: bainite), (c) weld area (B: bainite as the background microstructure), and (d) weld fusion line.

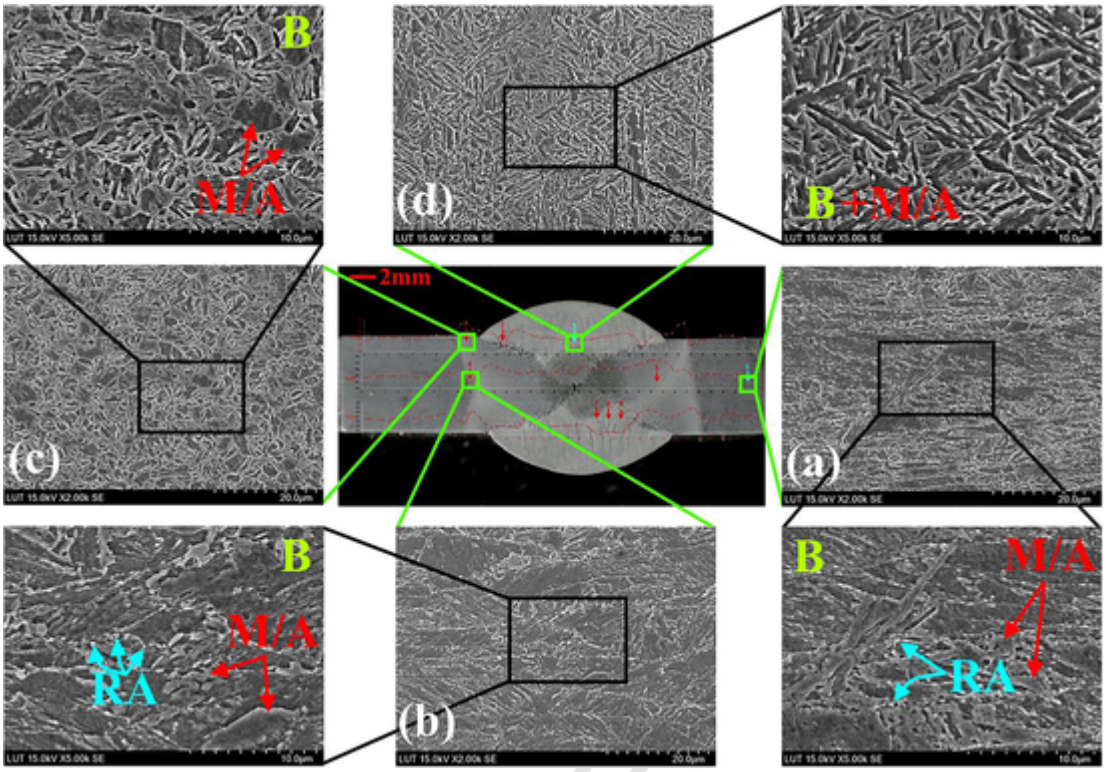

Fig. 13. SEM micrographs of S1100-HQ at: (a) BM (M/A: martensite-austenite islands, RA: retained austenite, B: bainite as the background microstructure), (b) softened HAZ, (c) HAZ with the hardness raise, and (d) weld filler material.

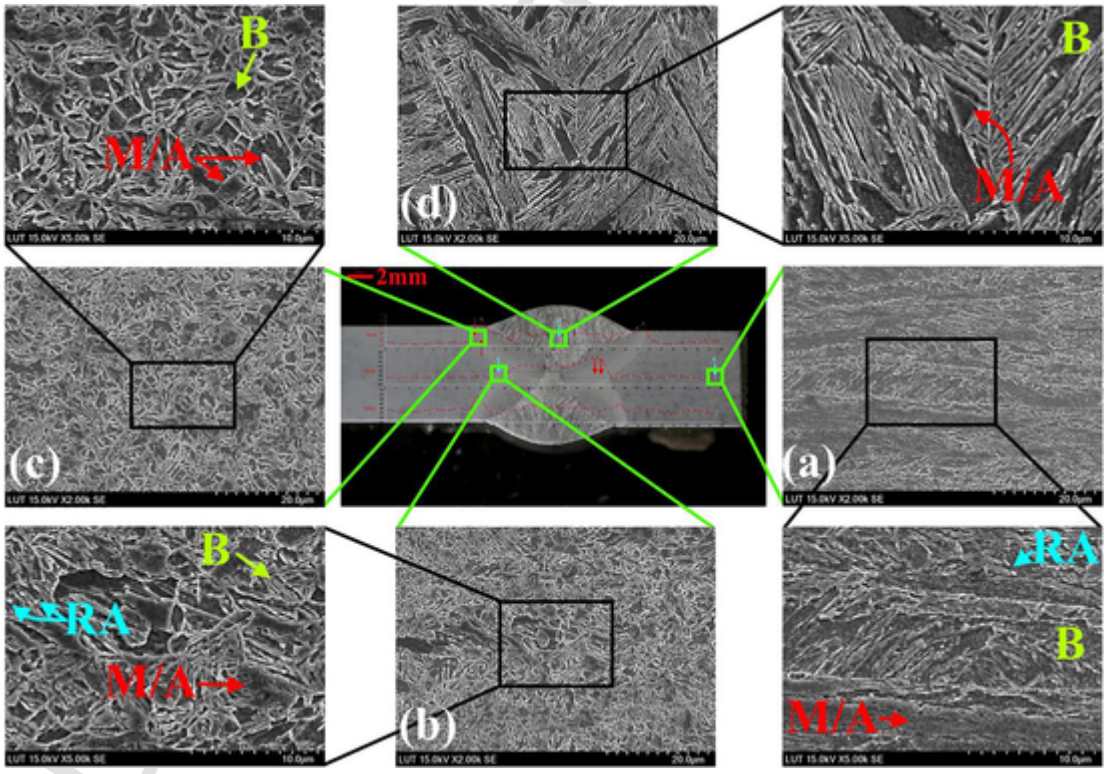

Fig. 14. SEM micrographs of S1100-LQ at: (a) BM (M/A: martensite-austenite islands, RA: retained austenite, B: bainite), (b) softened HAZ, (c) HAZ with the hardness raise, and (d) weld filler material.

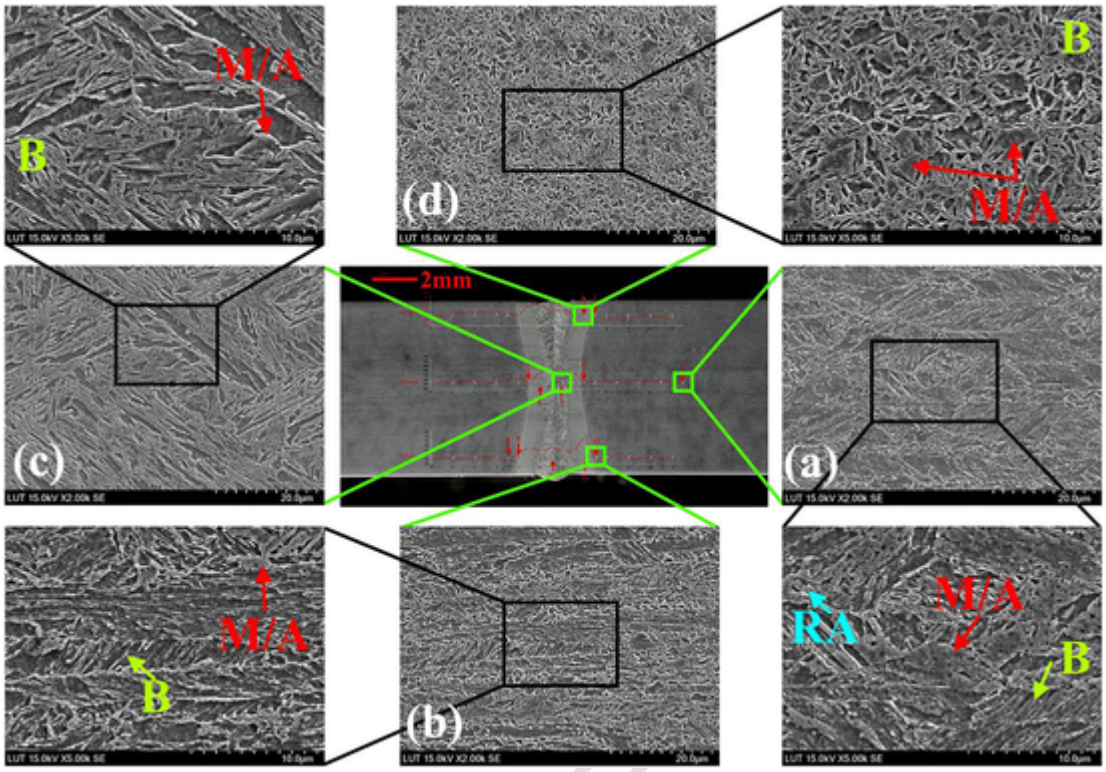

Fig. 15. SEM micrographs of S1100-LW at: (a) BM (M/A: martensite-austenite islands, RA: retained austenite, B: bainite), (b) softened HAZ, (c) weld area (bainite as the background microstructure), and (d) weld fusion line.

Since similar filler material is used to weld S960 and S1100 during the GMAW process, the fusion zones reveal the same microstructure which is a mixture of bainite and M/A. Fig. 15(c) shows that the LW specimen also has a similar microstructure at its fusion zone.

5. Conclusion

This paper dealt with the influence of HI on the mechanical properties of butt-welded high and ultra-high strength plates made of S700, S960 and S1100 steels. Both GMAW and laser welding were adopted. The welded plates were loaded to failure in tension, and micro-hardness measurements were performed at through the thickness of weldments. In addition, microstructure of the weldments were examined at different locations, especially at the softened HAZ. According to the results, following conclusions are made:

- Under the applied range of HI values, no major reduction in f_y and f_u of S700 and S1100 is noticeable. However, S960 shows reduction in both f_y and f_u as the magnitude of HI increases reaching maximum reduction values of 13% and 21%, respectively.
- Regardless of the welding HI, ε_y shows no major fluctuation. However, for all the weldments, ε_u, and elongation at break reduces as the welding HI increases, with S960 having the highest reduction. The laser-welded specimens show the best performance by reaching ductility of the BMs due to the very low HI values.
- The failure at the weldments of S700 and S1100 happened at the BM by the localization of shear bands in an inclined 30° angle of fracture. However, plastic strain localization at the HAZ of the S960 specimens led to failure at zero degree angle.
- The micro-hardness profiles of the welded specimens show softening to happen at the HAZ of all specimens. However, the S1100 steel plates have the least reductions, which was in the range of 4–11%, depending on the welding HI energy. The maximum reduction of the hardness values at the softened HAZ of S700 and S960 is 34% and 46%, respectively.
- The applicability of the available correlations between hardness and mechanical properties, f_y and f_u, were studied for the welded plates. Even though the current formulas by Murakami [39], and Pavlina & Van Tyne [40], provide a range in which the properties can fit within, yet due to the microstructural complexity of the studied BMs, the scatter data has a considerable range. More test data is required in order to establish an accurate correlation between hardness and mechanical properties, with the help of microstructure examination to provide insight into the phenomenon observed.
- The microstructure of the S700 at the HAZ shows appearance of granular bainite, which is a softer region compared to bainite and martensite, resulted in hardness drop at the softened HAZ.
- The welding HI seems to have a major impact on the microstructural features at the softened HAZ of S960. That is the reason why welded S960 specimens show various levels of hardness reduction. Besides, the sequence of welding passes has a considerable effect on the microstructural features of S960.
- Regardless of the welding process, the softened HAZ of all welded S1100 specimens are a combination of coarse bainite and martensite, which is similar to the BM's microstructure. The homogeneous microstructure of this steel resulted in the least hardness drop at the HAZ.

Acknowledgement

The authors would like to appreciate financial support of the Australian Research Council through a Discovery Project (DP150100442), Natural Science Foundation of China (51778457) and Business Finland through TuoTe project (23B25624YT10). The authors wish to thank SSAB Europe Co by providing the steel plates for this research. Special thanks to the technical support of the staff members at Laboratory of Steel Structures, Laboratory of Welding Technology and Laboratory of Laser Processing. The help and support of Mr. Matti Koskimäki in managing the laboratory work of this project is highly appreciated.

References

[1] H Tervo, A Kaijalainen, T Pikkarainen, S Mehtonen, D Porter. Effect of impurity level and inclusions on the ductility and toughness of an ultra-high-strength steel. Mater Sci Eng, A 2017;697:184–193.
[2] H Ban, G Shi. A review of research on high-strength steel structures. Struct Build 2018;171(8):625–641.
[3] X-L Zhao. Section capacity of very high strength (VHS) circular tubes under compression. Thin-Wall Struct 2000;37(3):223–240.
[4] H-T Li, B Young. Design of cold-formed high strength steel tubular sections undergoing web crippling. Thin-Wall Struct 2018;133:192–205.
[5] R Bjorhovde. Development and use of high performance steel. J Constr Steel Res 2004;60(3):393–400.
[6] P Graham. High strength steel use in Australia, Japan & the US. Struct Engineer 2006;84(21):27–31.
[7] X Lan, T-M Chan, B Young. Structural behaviour and design of chord plastification in high strength steel CHS X-joints. Constr Build Mater 2018;191:1252–1267.
[8] Shaw J, Kuriyama Y, Lambriks M. Achieving a lightweight and steel-intensive body structure for alternative powertrains. SAE technical paper no. 2011-01-0425; 2011.
[9] S Matsuku, K Hasegawa, Y Tanaka. Newly-developed ultra-high tensile strength steels with excellent formability and weldability. JFE Steel Corporation; 2007. Technical report no. 10.
[10] K Hasegawa, S Kaneko, K Seto. Cold-rolled and galvannealed (ga) high strength steel sheets for automotive cabin structure. JFE Steel Corporation; 2013. Technical report no. 18.
[11] J Kömi, P Karjalainen, D Porter. Direct-quenched structural steels. Encyclopedia of iron, steel, and their alloys; 2015. doi:10.1081/E-EISA-120049737.
[12] S Afkhami, T Björk, J Larkiola. Weldability of cold-formed high strength and ultra-high strength steels. J Constr Steel Res 2019;158:86–98.
[13] S Keeler, K Menachem, PJ Mooney. Today's AHSS. Advanced high strength steels application guidelines version 6.0. World Auto Steel; 2017. p. 12.
[14] BS EN 1993-1-12. Eurocode3: Design of steel structures: Part 1-12: additional rules for the extension of EN 1993 up to Steel Grades S700. London: BSI; 2007.
[15] ANSI/AISC 360-10. Specification for structural steel buildings. Chicago: American Institute of Steel Construction; 2010.
[16] M Amraei, M Dabiri, T Björk, T Skriko. Effects of workshop fabrication processes on the deformation capacity of S960 ultra-high strength steel. ASME J Manuf Sci Eng 2016;138(12). 121007–121007-13.
[17] DA Porter. Weldable high-strength steels: challenges and engineering applications. IIW international conference high-strength materials – challenges and applications, 2–3 July 2015, Helsinki, Finland; 2015.
[18] F Azhari, A Heidarpour, X-L Zhao, CR Hutchinson. Post-fire mechanical response of ultra-high strength (Grade 1200) steel under high temperatures: Linking thermal stability and microstructure. Thin-Wall Struct 2017;119:114–125.
[19] F Farrokhi, J Siltanen, A Salminen. Fiber laser welding of direct-quenched ultra-high strength steels: evaluation of hardness tensile strength, and toughness properties at subzero temperatures. ASME J Manuf Sci Eng 2015;137(6). pp. 061012-1(10).
[20] M Amraei, T Skriko, T Björk, X-L Zhao. Plastic strain characteristics of butt-welded ultra-high strength steel (UHSS). Thin-Wall Struct 2016;109:227–241.
[21] W Guo, D Crowther, JA Francis, A Thompson, Z Liu, L Li. Microstructure and mechanical properties of laser welded S960 high strength steel. Mater Des 2015;85:534–548.
[22] W Guo, L Li, S Dong, D Crowther, A Thompson. Comparison of microstructure and mechanical properties of ultra-narrow gap laser and gas-metal-arc welded S960 high strength steel. Opt Lasers Eng 2017;91:1–15.
[23] M Amraei, H Jiao, X-L Zhao, L-W Tong. Fatigue testing of butt-welded high strength square hollow sections strengthened with CFRP. Thin-Wall Struct 2017;120:260–268.
[24] J Siltanen, T Skriko, T Björk. Effect of the welding process and filler material on the fatigue behavior of 960 MPa structural steel at a butt joint configuration. J Laser Appl 2016;28(2):1–9.
[25] JH Lee, SH Park, HS Kwon, GS Kim, CS Lee. Laser, tungsten inert gas, and metal active gas welding of DP780 steel: comparison of hardness, tensile properties and fatigue resistance. Mater Des 2014;64:559–565. doi:10.1016/j.matdes.2014.0-7.065.
[26] MS Węglowski, M Zeman. Prevention of cold cracking in ultra-high strength steel Weldox 1300. Arch Civ Mech Eng 2014;14:417–424.
[27] K Wallin, S Pallaspuro, I Valkonen, P Karjalainen, P Suikkanen. Fracture properties of high performance steels and their welds. Eng Fract Mech 2015;135:219–231.
[28] S Pallaspuro, H Yu, A Kisko, D Porter, Z Zhang. Fracture toughness of hydrogen charged as-quenched ultra-high-strength steels at low temperatures. Mater Sci Eng, A 2017;688:190–201.
[29] LW Tong, LC Niu, S Jing, LW Ai, X-L Zhao. Low temperature impact toughness of high strength structural steel. Thin-Wall Struct 2018;132:410–420.
[30] H Jiao, X-L Zhao, A Lau. Hardness and compressive capacity of longitudinally welded very high strength steel tubes. J Constr Steel Res 2015;114:405–416.
[31] T Şükrü. The assessment of carbon equivalent formulas in predicting the properties of steel weld metals. Mater Des 2010;31(5):2649–2653.
[32] EN 1011-1. European Standard: Welding recommendations for welding of metallic materials Part 1: General guidance for arc welding. Brussels; 2009.
[33] F Javidan, A Heidarpour, X-L Zhao, CR Hutchinson, J Minkkinen. Effect of weld on the mechanical properties of high strength and ultra-high strength steel tubes in fabricated hybrid sections. Eng Struct 2016;118:16–27.
[34] EN 1011-2. European Standard: welding recommendations for welding of metallic materials Part 1: General guidance for arc welding. Brussels; 2001.
[35] L Anand, WA Spitzig. Initiation of localized shear bands in plain strain. J Mech Phys Solids 1980;28:113–128.
[36] H Jiao, X-L Zhao. Shear band orientation of very high strength (VHS) circular steel tubes. The third Australasian congress on applied mechanics, Sydney; 2002.
[37] T Björk, T Nykänen, I Valkonen. On the critical plane of axially loaded plate structures made of ultra-high strength steel. Weld World 2017;61:139–150.
[38] X Liu, K-F Chung, H-C Ho, M Xiao, Z-X Huo, DA Nethercot. Mechanical behavior of high strength S690-QT steel welded sections with various heat input energy. Eng Struct 2018;175:245–256.
[39] Y Murakami. Metal fatigue: effects of small defects and nonmetallic inclusions. 1st ed. Netherlands: Elsevier Science Ltd.; 2002. 390 p.
[40] EJ Pavlina, CJ Van Tyne. Correlation of yield strength and tensile strength with hardness for steels. J Mater Eng Perform 2008;17(1):888–893.
[41] A Navarro-López, J Hidalgo, J Sietsma, MJ Santofimia. Characterization of bainitic/martensitic structures formed in isothermal treatments below the Ms temperature. Mater Charact 2017;128:248–256.
[42] H Bhadeshia. Bainite in steels. Chapter 11: Other motphologies of bainite; 2015. p. 277.
[43] ZX Qiao, YC Liu, LM Yu, ZM Gao. Effect of cooling rate on microstructural formation and hardness of 30CrNi3Mo steel. Appl Phys A 2009;95:917–922.